



Assembly of graphene nanoflake-quantum dot hybrids in aqueous solution and their performance in light-harvesting applications

Antonio Attanzio,^{a,†} Martin Rosillo-Lopez,^{b,†} Andrea Zampetti,^c Ioannis Ierides,^c Franco Cacialli,^c Christoph G. Salzmann^{b,*} and Matteo Palma^{a,*}

Received 00th January 20xx,
Accepted 00th January 20xx

DOI: 10.1039/x0xx00000x

www.rsc.org/

Graphene nanoflakes and CdSe/ZnS quantum dots were covalently linked in environmentally friendly aqueous solution. Raman spectroscopy and photoluminescence studies, both in solution and on surfaces at the single nanohybrid level, showed evidence of charge transfer between the two nanostructures. The nanohybrids were further incorporated into solar cell devices, demonstrating their potential as light harvesting assemblies.

The combination of graphene and semiconducting nanocrystals (quantum dots, QDs) in functional heterostructures is attracting growing interest^{1–4} due to the tuneable emitting and efficient broadband light-harvesting properties of QDs, and the mechanical robustness and excellent charge transport properties of graphene. As new functionalities and enhanced photo-response properties can emerge at this organic-inorganic interface,^{5–7} QD-graphene nanohybrids have been employed for optoelectronic applications, including photodetectors,^{8,9} solar cells,^{10–13} and transistors,^{14,15} as well as for catalysis^{16–18} and sensing.¹⁹

Light-induced processes at the graphene-QD interface are governed by short-range electronic interactions, and strong electronic coupling between the two nanomoiety is desirable for the implementation of such nanostructures into devices. Evidence of electronic coupling in graphene-QD hybrids has been demonstrated, with both energy transfer^{20,21} and charge transfer^{14,15,22–24} being proposed as mechanisms for the deactivation of the excited state of the QDs. Such a variety of results and interpretations is mainly due to the

diversity of the systems investigated, e.g. the use of different graphene-based material [pure graphene, graphene oxide(GO) or reduced graphene oxide (rGO)], and the nature of the chemical interaction (covalent or non-covalent/electrostatic interactions) between the QDs and the nanocarbon sheets.

In this regard, one of the main challenges in working with graphene is its relatively inertness and low solubility which can result in issues in terms of assembly and processability; this is even more pronounced when employing water as a solvent, as the high degree of hydrophobicity of graphene promotes its aggregation and subsequent precipitation.²⁵ One of the most common routes to overcome such issues is the functionalization of graphene through the introduction of oxygen containing groups as defects on the sp² carbon network; this results in the formation of graphene oxide or reduced graphene oxide,^{1,26} that show a higher degree of dispersibility in aqueous solutions. However, such oxidation destroys some of the sp² graphenic character.²⁷ Moreover, even if in this way anchoring groups for the subsequent attachment of other components can be generated, this functionalisation is unspecific and uncontrolled, with defects on the graphene plane as well as at the edges. Previous work exploring non-covalent combinations of conjugated polymers and rGO, has for example demonstrated unexpected results in terms of lack of significant quenching of the conjugated fluorophore photoluminescence.²⁸

Here we present a facile assembly strategy in aqueous solution for the covalent attachment of CdSe/ZnS quantum dots to graphene edges. We employed carboxylated graphene nanoflakes (GNFs) characterized by the absence of defects on the basal sp² plane and a high density of carboxylic groups predominantly at the edges;^{29,30} these functionalities were exploited as anchoring groups for the tethering of QDs on the graphene edges. Evidence of electronic coupling between the two nanomoiety was demonstrated through stationary and time-resolved photoluminescence experiments, as well as *via* Raman spectroscopy-based investigations. Additionally, single-molecule measurements indicated a charge-transfer

^a School of Biological and Chemical Sciences, Materials Research Institute, Queen Mary University of London Mile End Road, London E14NS, UK. E-mail: m.palma@qmul.ac.uk

^b Department of Chemistry, University College London 20 Gordon Street, WC1H 0AJ, London, UK. E-mail: c.salzmann@ucl.ac.uk

^c Department of Physics and Astronomy and London Centre for Nanotechnology, University College London, London, WC1H 0AH, UK.

† These authors contributed equally.

Electronic Supplementary Information (ESI) available: [details of any supplementary information available should be included here]. See DOI: 10.1039/x0xx00000x

mechanism between the QD (acting as a donor) and the graphene (as the acceptor). This was further exploited for the fabrication of photovoltaic cells that exhibit improved photocurrents due to the graphene electron-acceptor nature favouring the charge-extraction processes from the photoexcited QDs.

Water-soluble and high-purity carboxylated graphene nanoflakes were prepared through oxidative break-down of multiwalled carbon nanotubes in a mixture of concentrated sulfuric acid and nitric acid, as previously reported^{29,30} [see also the Supporting Information (SI)]. These GNFs are characterized by a relatively low defect density on the graphene basal plane, while they show a high density of carboxyl groups along the edges (see Figure S1). It has been demonstrated that the carboxyl groups at the edges are in dynamic equilibrium with carboxylic anhydride groups in water, which exhibit a high reactivity towards nucleophilic attack at the carbonyl carbon atom and therefore offer themselves for straight-forward chemical functionalisation under mild conditions.³⁰

Taking advantage of this high reactivity, we employed commercially available, water-soluble amino-functionalized QDs, which can rapidly attack the C=O groups at the edges of the nanoflakes forming stable amide bonds. The formation of amide bonds between other amines and the carboxylic anhydride groups has been previously demonstrated through FTIR and zeta potential measurements;³⁰ we employed a similar strategy (see the SI) to covalently link QDs to the graphene nanoflakes edges, in environmentally-friendly and biocompatible aqueous solutions. Diluted GNF-QD nanohybrid solutions were cast onto highly-oriented pyrolytic graphite (HOPG) and imaged *via* atomic force microscopy (AFM). Figure 1 (see also Figure S2) shows a typical AFM image of GNF-QD nanohybrids: the QDs are surrounded by the flakes and in some cases the flakes are found to bridge several QDs into small clusters (see also Figure S3).

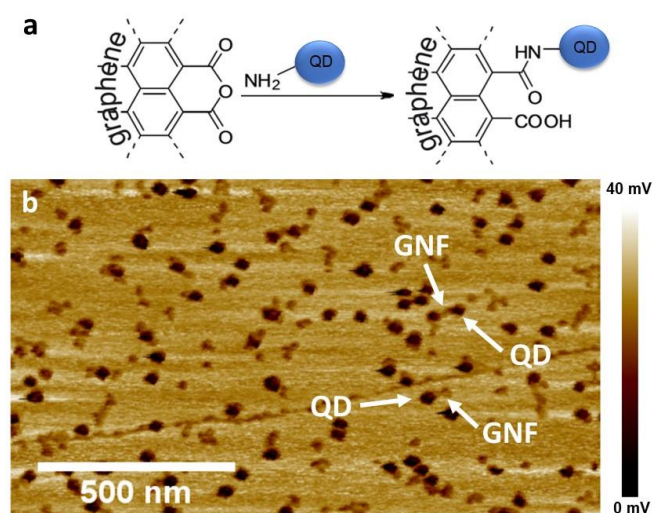


Figure 1: (a) Schematic illustration of the GNF-QD coupling chemistry. (b) Representative adhesion AFM image of the GNF-QD hybrids: the colour contrast is an indication of the different

mechanical response of the AFM tip to the two distinct nanomaterials forming the heterostructures (Z scale = 40 mV).

In order to demonstrate electronic coupling between the two nanomaterials forming the hybrids, we monitored the stationary photoluminescence of QDs by comparing solutions of pristine QDs and GNF-QD heterostructures (see the SI). A 93 % quenching of the stationary luminescence of the QDs was observed when attached to the GNF compared to pristine QDs (Figure 2a). This strongly indicates the occurrence of electronic coupling between the two nanomaterials, as previously shown in similar systems³¹ and ascribed to either energy transfer²⁰ or charge transfer.²³

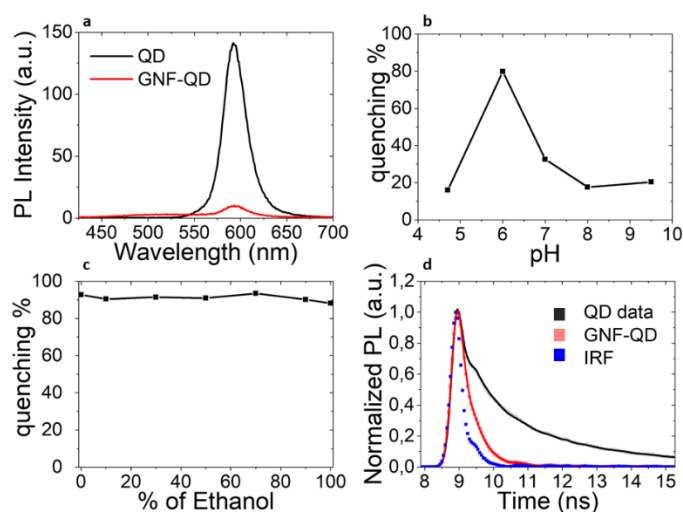


Figure 2: (a) Stationary Photoluminescence spectra of QD (black) and GNF-QD hybrids (red). The spectrum of the GNF-QD hybrids shows a weak shoulder centred at around 515 nm which is due to the luminescence of the nanoflakes themselves. Photoluminescence quenching of GNF-QD hybrids at different (b) pH and (c) solvent polarity. (d) Time-resolved photoluminescence spectra of QDs (black) and GNF-QD hybrids (red). Samples were excited at 420 nm, the emission was recorded at 594 nm. Table 1 shows the fitting parameters of the biexponential decay taking into account the instrument response function (IRF) (blue dots).

We further studied how the change of pH (employing different buffers: see the SI) and the polarity of the solvent (different % of ethanol/water solutions) affect the amide bond formation; this was achieved by monitoring the extent of the QD photoluminescence quenching in the hybrids (Figure 2b,c). We observed a maximum PL quenching at pH 6 (80 %), and a 33% quenching at pH 7; the QD PL in the hybrids was quenched of only ca. 20 % in the other pH conditions investigated (pH ranging from 4 to 9.5). Differently, only slight variations were observed when the polarity of the solvent employed was altered.

The change of quenching with the pH, as well as the lack of any significant differences with solvent polarity, can be explained in terms of the covalent bond formation between the QDs and the

GNFs: pH can have a deep influence on the covalent bond formation, in particular it is a key parameter for the stabilization of the various charged intermediates. If the pH is too low, all the amino groups are protonated, thereby hampering the nucleophilic attack on the carbonyl and lowering the reaction yield; on the other hand, a high pH promotes the OH⁻ catalysed hydrolysis of the anhydride, thereby favouring the formation of less reactive carboxylate groups, hence lowering the yield of the reaction.^{32–34} In our system, the best conditions were obtained around pH 6, where the highest degree of quenching (80%) was observed.³⁵ Moreover, the lack of any significant changes in the quenching of the QD emission, when the polarity of the solvent is changed, supports the generation of a covalent bond rather than an electrostatic interaction, as only in the latter case a different distribution of the charges at the interface, induced by the solvent polarity, could potentially affect the GNF-QD interactions and the QD emission in the hybrids.

Time-resolved measurements were carried out in order to study the decay dynamics of the excited QD in the hybrids: Figure 2d compares the emission decay traces for pristine QD and GNF-QD hybrids.³⁶ Pristine QDs are characterized by a typical biexponential decay where the shorter lifetime ($t_1 = 0.83$ ns) accounts for the emissive recombination of internal core states, while the longer one ($t_2 = 3.23$ ns) accounts for the radiative recombination of excitons involving surface states (Table 1).³⁷ The two processes contribute almost equally to the total PL with 53 % of the total emission related to the core states emission and the remaining 47 % contribution from the surface related emission. In the case of the GNF-QD hybrids a shortening of both short and long lifetimes (Table 1, $t_1 = 0.13$ ns and $t_2 = 0.50$ ns) was observed while the PL decay followed a nearly monoexponential decay with 86 % of the emission due to the core recombination processes. The reduction of the total lifetime, together with the increase of the contribution of the faster component to the total emission, is an indication of charge transfer occurring in our hybrids, as previously described for similar heterostructures:^{31,38,39} Since short-range charge transfer involves mainly surface states, a reduction in amplitude of the surface state emission kinetics (t_2) is expected, with the decay evolving from a biexponential to a nearly monoexponential one. Conversely, energy transfer is a long-range process involving both core and surface states, and would affect both the lifetimes preserving a biexponential decay.³⁸ Additionally, upon changing pH and solvent polarity, the fitting parameters of the decay dynamics are in line with the observed PL quenching and aforementioned charge transfer rationalization: see Figure S4.⁴⁰

Table 1: Fitting parameters of the photoluminescence decay traces of pristine QD and GNF-QD hybrids. The decays were fitted to a biexponential function: $PL(t) = a_1 e^{-\frac{t}{\tau_1}} + a_2 e^{-\frac{t}{\tau_2}}$ (see also the SI).

Sample	a_1	t_1 (ns)	t_2 (ns)
QD	0.53	0.83	3.23
GNF-QD	0.86	0.13	0.50

Charge-transfer events can alter the carrier concentration and mobility within the graphene, with the effect of shifting the Fermi energy and therefore changing the electronic and optical properties of the material.^{41–43} Significant modifications in the properties of graphene, especially its phonon spectrum and electronic structure, have been reported to occur when electrons or holes are introduced by electrochemical means.^{44–47} Therefore, in order to investigate the effect of QDs on the electronic structure of the graphene nanoflakes, we studied the nanohybrids via Raman spectroscopy (see the SI and Figure S6).

Figure 3 shows the characteristic G and D bands for the pristine graphene (black curve) at 1387 and 1604 cm⁻¹ respectively. The relatively broad peaks compared to large-sheet graphene arise from the nanoscale dimensions of the GNFs.^{27,29,30} The G and D peaks are also presented in the spectrum of the hybrids, but the D peak is down-shifted by 18 cm⁻¹ while the G peak is down shifted by 15 cm⁻¹. The observed down shift of the G and D bands of the GNF compared to the pristine graphene indicates that the electronic levels in graphene are perturbed by the presence of the QD suggesting a strong coupling between the two nanomaterials.⁴⁸ This confirms the nature of the covalent bond, as only a strong overlap of electronic orbitals can cause such a perturbation which is not expected for weak (e.g. electrostatic) interactions. Moreover, a down shift of the Raman features can be ascribed to electron transfer from the photoexcited QD to the nanoflakes, as previously observed for graphene^{46,47} and single-walled carbon nanotubes doped with electron donor compounds⁴⁹ which transfer electrons to the carbon π^* states. These findings are in agreement with the time-resolved data, suggesting charge-transfer events between the QDs and GNFs as a deactivation pathway for the QD excited states, where electrons are injected from the photoexcited QDs into the graphene.

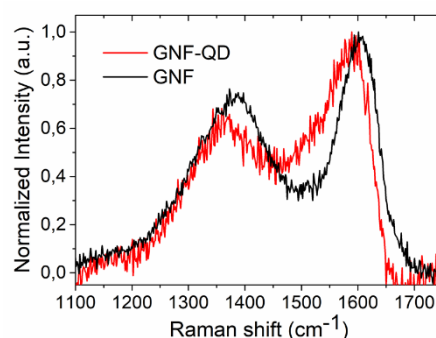


Figure 3: Raman spectra (514.5 nm) of pristine graphene nanoflakes (black) and GNF-QD hybrids (red).

To investigate further the nature of the electronic coupling between the two nanostructures, we carried out PL studies of individual nanostructures with single particle control. We cast diluted solutions on glass substrates in order to obtain physisorbed structures spaced at least 1 μm apart, hence optically resolvable (see Figure S7). Quantum dots exhibit dynamic fluctuation of fluorescence intensity (i.e. “blinking”),⁵⁰ which is usually indicative of single emission

behaviour.^{51,52} The bright states (ON states) correspond to the radiative recombination of photo-generated electron-hole pairs, while the states with no luminescence (OFF states) correspond to a non-radiative Auger-mediated recombination which results in the ejection of charges from the nanocrystal leaving it in a charged 'dark' state.

Representative fluorescence intensity traces of a single pristine QD and a single GNF-QD hybrid are shown in Figure 4a,c, respectively; the histograms of the normalised fluorescence intensity of the corresponding cumulative data for over 30 single dots are plotted in Figure 4b,d. In both cases, there is a bimodal distribution of the intensities where the high-intensity peak is related to the QD in the ON states while the low intensity peak is linked to those in the OFF states. The observed fluorescence intensity traces, as well as the histograms of the PL intensities, of pristine QD exhibit a different behaviour from the QD functionalized with GNF. Although in both cases the histograms are characterized by two peaks of ON and OFF states, pristine QDs are characterized by an almost equal occurrence of the two states, while in the case of the hybrids the histogram as well as the single trace show a clear prevalence of the OFF states over the ON states. This indicates that the blinking behaviour is affected by the presence of the GNFs, which deeply influence the excitation recombination processes in the QDs: a charge ejection process would increase the probability density of the OFF states leaving the nanoparticles in a charged, "dark state", for longer periods of time.

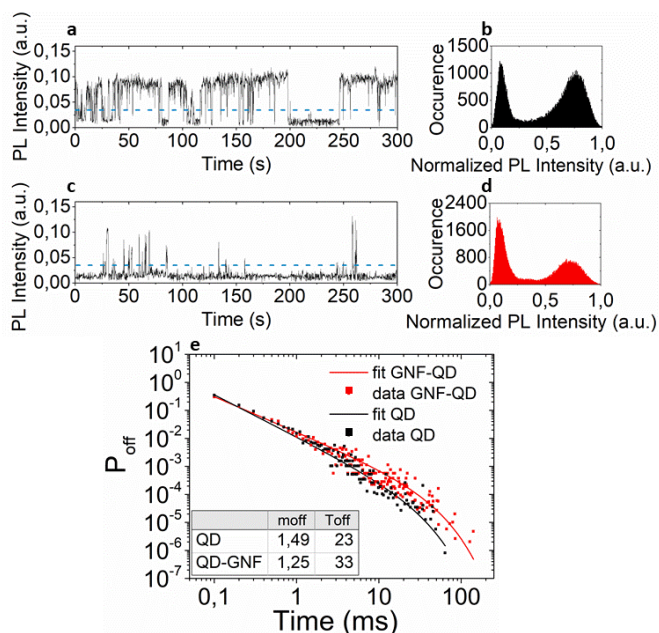


Figure 4: Typical fluorescence intensity traces of representative samples of (a) pristine QDs and (c) GNF-QD hybrids. Fluorescence intensity histograms were obtained by cumulating over 30 traces for (c) individual QDs and (d) GNF-QD hybrids. (e) Probability density of OFF states constructed from over 30 single QDs (black) and GNF-QD hybrids (red). Solid lines are best fit to a truncated power law (see the SI).

By selecting a threshold (blue dotted lines in Figure 4a,c) it is possible to discriminate between "ON" and "OFF" periods, and for each time bin a probability of OFF states can be calculated (see the SI). The probability distributions of the OFF periods (P_{OFF}) for the QDs and the GNF-QD nanostructures are shown in Figure 4e, confirming the different blinking behaviour. Both the QDs and the GNF-QD heterostructures show a power-law distribution, but deviate from this distribution at longer times, as previously reported by other groups.^{53,54} This distribution can be fitted by a truncated power law (equation 4 in SI; the typical exponent for this type of QD is reported to be between 1.5 and 1.7.^{55,56} The calculated values of the exponents for pristine QDs and the GNF-QD hybrids are 1.49 and 1.25, respectively. The smaller power law exponent (m_{OFF} in Table in Figure 4e; see the SI) indicates an increased probability density of longer OFF events, as previously described for similar donor-acceptor systems,^{31,53,54} and further confirms charge transfer process as the deactivation pathway of photoexcited QDs.^{41–43}

In order to exploit this charge-transfer process occurring at the GNF-QD interface, we fabricated solution-processable solar cell devices where GNF-QD hybrids were employed as the active component on TiO₂ photoanodes. The device schematic is shown in Figure 5a and consists of a TiO₂ electrode, where the GNF-QD hybrids have been deposited, acting as the photoactive anode, and a platinum counter electrode separated by a Na₂S electrolyte solution.

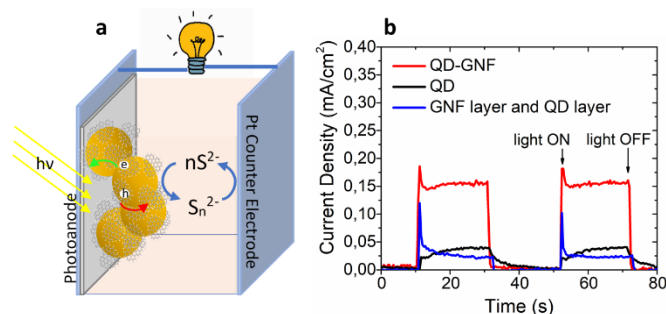


Figure 5: (a) Schematic illustration of the solar cell configuration, (b) photocurrent response of QDs and GNF-QD hybrids to ON/OFF illumination.

We carried out photocurrent measurements with the solar cells during ON/OFF cycles of illumination; for all devices we measured a constant value of the current during the periods of illumination confirming the stability of the devices and lack of degradation during the measurements. Furthermore, we observed a substantial increase (more than 3 times) of the photocurrent response when the TiO₂ was sensitized with our GNF-QD hybrids compared to only QDs, as shown in Figure 5b. One of the key steps for solar cell efficiency is the charge-extraction process from the QDs into the TiO₂, and we propose that in our case the presence of the GNF increases the extent of this process thereby providing higher generated currents compared to the QD-only device, as previously reported for similar graphene based devices^{23,57–59} as well as C₆₀⁶⁰ and CNTs.⁶¹ While higher photocurrent responses have been previously reported under

controlled atmosphere (Ar gas),⁵⁸ our results in ambient conditions are comparable to other studies performed with similar materials but processed from organic solutions.^{23,62} Notably, our device is fabricated from environmentally friendly aqueous solutions, while additionally allowing for single-molecule control of the organic-inorganic interface.

As a control experiment, we prepared solar cells where first a GNF layer was deposited on the TiO₂ anode followed by a deposition of a QDs layer (blue curve in Figure 5b). In this case, a simple physisorption of the QDs on the GNFs can be expected with minimal linking at the interface, and we observed no significant variations of the photo-generated current compared to the devices with only QDs. This indicates that in the absence of extensive covalent bonds between the two components, the electronic coupling is not strong enough to enhance the charge extraction from the QDs, resulting in no improvement in the generated photocurrent.

Conclusions

In conclusion, we have presented a facile and green assembly strategy for the formation of GNF-QD nanohybrids in aqueous solution, where graphene nanoflakes have been covalently attached to quantum dots. Photoluminescence studies of the GNF-QD hybrids, in solution and on surface with single particle control, show evidence of strong coupling between the two nanomaterials, suggesting that a charge transfer mechanism is responsible for the deactivation of the excited QDs. This was further explored by Raman spectroscopy, which confirmed strong charge transfer processes taking place between the excited QD and the graphene. Finally, we exploited this charge transfer in solar cell devices, that exhibited improved photocurrents compared to a QD-only device, demonstrating the potential of GNF-QD nanohybrids as light-harvesting assemblies.

To the best of our knowledge this is the first fully water-based assembly of graphene-QD hybrids with evidence of charge transfer process at the single nanohybrid level, and further implementation in a solar cell device. This environmentally-friendly and biocompatible strategy holds great potential for scalable and green manufacturing, as well as for bioelectronics. Future investigations will explore the tunability of the electronic coupling⁶¹ at the graphene-nanocrystal interface, via the use of ligands of different length and chemical nature, bridging the QDs and the GNFs in the hybrids.

Acknowledgements

The authors gratefully acknowledge funding by: the Engineering and Physical Sciences Research Council under Award EP/M029506/1; the European Community's Seventh Framework Programme (FP7/2007-2013) ITN MSCA action under Grant Agreement No. 607585 (OSNIRO). FC is a Royal Society Wolfson Merit Award holder. CGS thanks the Royal Society for a University Research Fellowship (UF150665). CGS & MRL have received funding from the European Research Council (ERC) under the European Union's Horizon 2020

research and innovation programme (grant agreement No 725271). It was supported by the EPSRC Centre for Doctoral Training in Advanced Characterisation of Materials (grant number EP/L015277/1). The authors acknowledge Dr Vicente Araullo-Peters and the NanoVision center at Queen Mary University of London for TEM measurements.

Conflicts of interest

There are no conflicts to declare.

Notes and references

- 1 C. J. Shearer, A. Cherevan and D. Eder, *Adv. Mater.*, 2014, **26**, 2295–2318.
- 2 L. Tong, F. Qiu, T. Zeng, J. Long, J. Yang, R. Wang, J. Zhang, C. Wang, T. Sun and Y. Yang, *RSC Adv.*, 2017, **7**, 47999–48018.
- 3 A. Cao, Z. Liu, S. Chu, M. Wu, Z. Ye, Z. Cai, Y. Chang, S. Wang, Q. Gong and Y. Liu, *Adv. Mater.*, 2010, **22**, 103–106.
- 4 N. Li, M. Cao and C. Hu, *Nanoscale*, 2012, **4**, 6205.
- 5 A. K. Geim, *Science*, 2009, **324**, 1530–1534.
- 6 A. C. Ferrari, F. Bonaccorso, V. Fal'ko, K. S. Novoselov, S. Roche, P. Bøggild, S. Borini, F. H. L. Koppens, V. Palermo, N. Pugno, J. A. Garrido, R. Sordan, A. Bianco, L. Ballerini, M. Prato, E. Lidorikis, J. Kivioja, C. Marinelli, T. Ryhänen, A. Morpurgo, J. N. Coleman, V. Nicolosi, L. Colombo, A. Fert, M. Garcia-Hernandez, A. Bachtold, G. F. Schneider, F. Guinea, C. Dekker, M. Barbone, Z. Sun, C. Galiotis, A. N. Grigorenko, G. Konstantatos, A. Kis, M. Katsnelson, L. Vandersypen, A. Loiseau, V. Morandi, D. Neumaier, E. Treossi, V. Pellegrini, M. Polini, A. Tredicucci, G. M. Williams, B. Hee Hong, J.-H. Ahn, J. Min Kim, H. Zirath, B. J. van Wees, H. van der Zant, L. Occhipinti, A. Di Matteo, I. A. Kinloch, T. Seyller, E. Quesnel, X. Feng, K. Teo, N. Rupesinghe, P. Hakonen, S. R. T. Neil, Q. Tannock, T. Löfwander and J. Kinaret, *Nanoscale*, 2015, **7**, 4598–4810.
- 7 T.-F. Yeh, C.-Y. Teng, L.-C. Chen, S.-J. Chen and H. Teng, *J. Mater. Chem. A*, 2016, **4**, 2014–2048.
- 8 Z. Sun, Z. Liu, J. Li, G. A. Tai, S. P. Lau and F. Yan, *Adv. Mater.*, 2012, **24**, 5878–5883.
- 9 Y.-L. Sun, D. Xie, M.-X. Sun, C.-J. Teng, L. Qian, R.-S. Chen, L. Xiang and T.-L. Ren, *Sci. Rep.*, 2018, **8**, 5107.
- 10 J. G. Radich, R. Dwyer and P. V. Kamat, *J. Phys. Chem. Lett.*, 2011, **2**, 2453–2460.
- 11 Y. Sun, Q. Wu and G. Shi, *Energy Environ. Sci.*, 2011, **4**, 1113.
- 12 Q. Chang, Z. Ma, J. Wang, P. Li, Y. Yan, W. Shi, Q. Chen, Y. Huang and L. Huang, *Energy Technol.*, 2016, **4**, 256–262.
- 13 F. Bonaccorso, L. Colombo, G. Yu, M. Stoller, V. Tozzini, A. C. Ferrari, R. S. Ruoff and V. Pellegrini, *Science*, 2015, **347**, 6217.
- 14 G. Konstantatos, M. Badioli, L. Gaudreau, J. Osmond, M. Bernechea, F. P. G. De Arquer, F. Gatti and F. H. L. Koppens, *Nat. Nanotechnol.*, 2012, **7**, 363–368.
- 15 A. V. Klekachev, M. Cantoro, M. H. Van Der Veen, A. L.

- Stesmans, M. M. Heyns and S. De Gendt, *Phys. E Low-Dimensional Syst. Nanostructures*, 2011, **43**, 1046–1049.
- 16 Y. Bu, Z. Chen, W. Li and B. Hou, *ACS Appl. Mater. Interfaces*, 2013, **5**, 12361–12368.
- 17 D. Chen, H. Zhang, Y. Liu and J. Li, *Energy Environ. Sci.*, 2013, **6**, 1362.
- 18 F. X. Xiao, J. Miao and B. Liu, *J. Am. Chem. Soc.*, 2014, **136**, 1559–1569.
- 19 W. Guo, S. Xu, Z. Wu, N. Wang, M. M. T. Loy and S. Du, *Small*, 2013, **9**, 3031–3036.
- 20 Z. Chen, S. Berciaud, C. Nuckolls, T. F. Heinz and L. E. Brus, *ACS Nano*, 2010, **4**, 2964–8.
- 21 F. Federspiel, G. Froehlicher, M. Nasilowski, S. Pedetti, A. Mahmood, B. Doudin, S. Park, J.-O. Lee, D. Halley, B. Dubertret, P. Gilliot and S. Berciaud, *Nano Lett.*, 2015, **15**, 1252–8.
- 22 C. X. Guo, H. Bin Yang, Z. M. Sheng, Z. S. Lu, Q. L. Song and C. M. Li, *Angew. Chemie - Int. Ed.*, 2010, **49**, 3014–3017.
- 23 I. V. Lightcap and P. V. Kamat, *J. Am. Chem. Soc.*, 2012, **134**, 7109–7116.
- 24 B. S. Kim, D. C. J. Neo, B. Hou, J. B. Park, Y. Cho, N. Zhang, J. Hong, S. Pak, S. Lee, J. I. Sohn, H. E. Assender, A. A. R. Watt, S. Cha and J. M. Kim, *ACS Appl. Mater. Interfaces*, 2016, **8**, 13902–13908.
- 25 G. Bepete, E. Anglaret, L. Ortolani, V. Morandi, K. Huang, A. Pénicaud and C. Drummond, *Nat. Chem.*, 2017, **9**, 347–352.
- 26 J. Liu, J. Tang and J. J. Gooding, *J. Mater. Chem.*, 2012, **22**, 12435.
- 27 M. Rosillo-Lopez and C. G. Salzmann, *Carbon N. Y.*, 2016, **106**, 56–63.
- 28 P. Li, F. Di Stasio, G. Eda, O. Fenwick, S. O. McDonnell, H. L. Anderson, M. Chhowalla and F. Cacialli, *ChemPhysChem*, 2015, **16**, 1258–1262.
- 29 C. G. Salzmann, V. Nicolosi and M. L. H. Green, *J. Mater. Chem.*, 2010, **20**, 314–319.
- 30 M. Rosillo-Lopez, T. J. Lee, M. Bella, M. Hart and C. G. Salzmann, *RSC Adv.*, 2015, **5**, 104198–104202.
- 31 A. Attanzio, A. Sapelkin, F. Gesuele, A. van der Zande, W. P. Gillin, M. Zheng and M. Palma, *Small*, 2017, **13**, 1603042.
- 32 P. J. Butler, J. I. Harris, B. S. Hartley and R. Leberman, *Biochem. J.*, 1969, **112**, 679–89.
- 33 R. Bott, *Bioconjugate Techniques*, Elsevier, 2014.
- 34 P. Yurkanis Bruice, *Organic Chemistry, 5th Edition*, Pearson.
- 35 When there is no pH control over the course of the reaction, as in the case of the normal coupling conditions in water, we assume the pH adjusts naturally around the optimum pH conditions as no acid or basic sub products are generated during the amide bond formation.
- 36 TRPL was carried out also for the emission peak of the GNF at 515 nm, but no difference was observed in the decays of pristine GNF and GNF-QD hybrids.
- 37 X. Wang, L. Qu, J. Zhang, X. Peng and M. Xiao, *Nano Lett.*, 2003, **3**, 1103–1106.
- 38 X. Peng, J. a Misewich, S. S. Wong and M. Y. Sfeir, *Nano Lett.*, 2011, **11**, 4562–8.
- 39 S. Kaniyankandy, S. Rawalekar and H. N. Ghosh, *J. Phys. Chem. C*, 2012, **116**, 16271–16275.
- 40 Concentration dependent investigations showed the expected trend in coupling: see figure S5.
- 41 L. M. Malard, M. A. Pimenta, G. Dresselhaus and M. S. Dresselhaus, *Phys. Rep.*, 2009, **473**, 51–87.
- 42 A. C. Ferrari, *Solid State Commun.*, 2007, **143**, 47–57.
- 43 A. C. Ferrari and D. M. Basko, *Nat. Nanotechnol.*, 2013, **8**, 235–246.
- 44 J. Yan, Y. Zhang, P. Kim and A. Pinczuk, *Phys. Rev. Lett.*, 2007, **98**, 1–4.
- 45 A. Das, S. Pisana, B. Chakraborty, S. Piscanec, S. K. Saha, U. V. Waghmare, K. S. Novoselov, H. R. Krishnamurthy, A. K. Geim, A. C. Ferrari and A. K. Sood, *Nat. Nanotechnol.*, 2008, **3**, 210–215.
- 46 B. Das, R. Voggu, C. S. Rout and C. N. R. Rao, *Chem. Commun.*, 2008, 5155–5157.
- 47 H. Liu, Y. Liu and D. Zhu, *J. Mater. Chem.*, 2011, **21**, 3335–3345.
- 48 G. B. Markad, S. Battu, S. Kapoor and S. K. Haram, *J. Phys. Chem. C*, 2013, **117**, 20944–20950.
- 49 A. M. Rao, P. C. Eklund, S. Bandow, A. Thess and R. E. Smalley, *Nature*, 1997, **388**, 257–259.
- 50 M. Nirmal, B. O. Dabbousi, M. G. Bawendi, J. J. Macklin, J. K. Trautman, T. D. Harris and L. E. Brus, *Nature*, 1996, **383**, 802–804.
- 51 C. Galland, Y. Ghosh, A. Steinbrück, M. Sykora, J. A. Hollingsworth, V. I. Klimov and H. Htoon, *Nature*, 2011, **479**, 203–207.
- 52 A. L. Efros and D. J. Nesbitt, *Nat. Nanotechnol.*, 2016, **11**, 661–671.
- 53 S. Jin and T. Lian, *Nano Lett.*, 2009, **9**, 2448–2454.
- 54 Z. Xu and M. Cotlet, *Small*, 2012, **8**, 253–258.
- 55 J. Abramson, M. Palma, S. J. Wind and J. Hone, *Adv. Mater.*, 2012, **24**, 2207–2211.
- 56 K. Shimizu, R. Neuhauser, C. Leatherdale, S. Empedocles, W. Woo and M. Bawendi, *Phys. Rev. B*, 2001, **63**, 1–5.
- 57 Q. Wu, H. Zhao, F. Huang, J. Hou, H. Cao, Z. Liu, S. Peng and G. Cao, *J. Phys. Chem. C*, 2017, **121**, 18430–18438.
- 58 N. Zhu, K. Zheng, K. J. Karki, M. Abdellah, Q. Zhu, S. Carlson, D. Haase, K. Židek, J. Ulstrup, S. E. Canton, T. Pullerits and Q. Chi, *Sci. Rep.*, 2015, **5**, 1–14.
- 59 M.-H. Jung and M.-J. Chu, *Nanoscale*, 2014, **6**, 9241–9.
- 60 P. Brown and P. V. Kamat, *J. Am. Chem. Soc.*, 2008, **130**, 8890–8891.
- 61 I. Robel, B. a. Bunker and P. V. Kamat, *Adv. Mater.*, 2005, **17**, 2458–2463.
- 62 S. Krishnamurthy and P. V. Kamat, *ChemPhysChem*, 2014, **15**, 2129–2135.
- 63 M. Freeley, A. Attanzio, A. Ceconello, G. Amoroso, P. Clement, G. Fernandez, F. Gesuele and M. Palma, *Adv. Sci.*, 2018, 1800596.